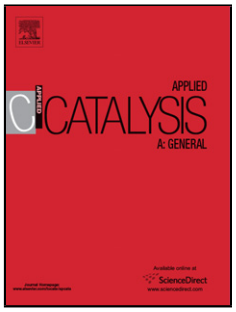

Title: Study of the electrical and catalytic properties of spinels
with $CuFe_{2-x}Mn_xO_4$ composition (x = 0, 0.4, 0.8, 1.6 and 2)

Author: Ionel Popescu Amel Boudjemaa Nassima Helaili
Yassine Bessekhouad Mădălina Tudorache Khaldoun Bachari
Ioan-Cezar Marcu

PII:	S0926-860X(14)00610-3
DOI:	http://dx.doi.org/doi:10.1016/j.apcata.2014.09.048
Reference:	APCATA 15029
To appear in:	*Applied Catalysis A: General*
Received date:	22-7-2014
Revised date:	24-9-2014
Accepted date:	27-9-2014

Please cite this article as: I. Popescu, A. Boudjemaa, N. Helaili, Y. Bessekhouad, M. Tudorache, K. Bachari, I.-C. Marcu, Study of the electrical and catalytic properties of spinels with $CuFe_{2-x}Mn_xO_4$ composition (x = 0, 0.4, 0.8, 1.6 and 2), *Applied Catalysis A, General* (2014), http://dx.doi.org/10.1016/j.apcata.2014.09.048

Dedicated to Jacques Védrine.

Study of the electrical and catalytic properties of spinels with $CuFe_{2-x}Mn_xO_4$ composition (x = 0, 0.4, 0.8, 1.6 and 2)

Ionel Popescu,[a] Amel Boudjemaa,[b] Nassima Helaili,[b,c] Yassine Bessekhouad,[c, d] Mădălina Tudorache,[e] Khaldoun Bachari,[b] Ioan-Cezar Marcu,[a, e, *]

[a] Research Center for Catalysts and Catalytic Processes, Faculty of Chemistry, University of Bucharest, 4-12, Blv. Regina Elisabeta, 030018 Bucharest, Romania

[b] Research Center in Analytical Chemistry and Physics (CRAPC), BP 248, Algiers RP 16004, Algeria

[c] Laboratory of Storage and Valorization of Renewable Energies, Faculty of Chemistry, U.S.T.H.B., BP 32, 16111 El-Alia, Algiers, Algeria

[d] National Veterinary School, BP 161 El-Harrach, Algiers, Algeria

[e] Laboratory of Chemical Technology and Catalysis, Department of Organic Chemistry, Biochemistry and Catalysis, Faculty of Chemistry, University of Bucharest, 4-12, Blv. Regina Elisabeta, 030018 Bucharest, Romania

Abstract

$CuFe_{2-x}Mn_xO_4$ spinels (x = 0, 0.4, 0.8, 1.6 and 2) were used as catalysts for the total oxidation of methane in the temperature range 450-800 °C and characterized by *in situ* electrical conductivity measurements. Their electrical conductivity was studied as a function of temperature and oxygen partial pressure and temporal responses during sequential exposures to air, methane – air mixture (reaction mixture) and pure methane in conditions similar to those of catalysis were analyzed. The catalytic activity decreased with increasing the value of x in the $CuFe_{2-x}Mn_xO_4$ spinels as follows: $CuFe_2O_4 > CuFe_{1.6}Mn_{0.4}O_4 > CuFe_{1.2}Mn_{0.8}O_4 > CuFe_{0.4}Mn_{1.6}O_4 > CuMn_2O_4$. $CuFe_2O_4$ appeared to be a p-type semiconductor while $CuMn_2O_4$ a n-type semiconductor under air in the reaction temperature range but $CuFe_2O_4$ became n-type while $CuMn_2O_4$ p-type when contacted

---

[*] Corresponding author. Tel.: +40 213051464; fax: +40 213159249. E-mail addresses: ioancezar.marcu@g.unibuc.ro ; ioancezar_marcu@yahoo.com

with methane. Both types of conduction mechanisms are present in $CuFe_{2-x}Mn_xO_4$ spinels with x = 0.4, 0.8 and 1.6, being predominant one or another as a function of temperature. Nevertheless, they were of p-type under air in the reaction temperature range and became of n-type when contacted with methane. The conducting behavior and redox properties of the spinels in the reaction temperature range were correlated with their catalytic behavior. For $CuMn_2O_4$ catalyst the reaction mainly involves surface lattice O^- species, whereas for the other surface lattice O^{2-} anions are mainly involved. In all cases the overall reaction mechanism can be assimilated to a Mars and van Krevelen mechanism.

Keywords: electrical conductivity; $CuFe_{2-x}Mn_xO_4$ spinels; methane combustion

1. INTRODUCTION

The most widely used catalysts for volatile organic compounds (VOCs) abatement are noble metals, generally supposed to be more active than metal oxides [1]. Nevertheless they have some disadvantages like high sintering rates, volatility, poisoning in the presence of water or sulfur compounds and high price [2]. Transition metal oxides which possess high chemical and thermal stability, resistance to poisoning and low costs become very attractive to obtain active oxidation catalysts of VOCs [3]. Moreover, it was already shown [1] that metal oxides can compete with noble metals in terms of catalytic performances. Therefore, in recent years, many efforts were directed towards the design of catalytic materials based on transition-metal oxides to replace noble metal catalysts for VOCs abatement [4-17]. In that context, several studies showed that spinel ferrites could be effective catalysts for the total oxidation of VOCs [18-24].

Ferrites are potential catalysts for this reaction due to their redox activity and their stability under oxidative conditions [25]. A spinel-type ferrite structure presents two types of interstitial sites, tetrahedral and octahedral, surrounded by four and six oxygen atoms, respectively [26]. The formula of the spinel ferrites is AB_2O_4 where the A^{II} ions occupy the tetrahedral and B^{III} ions the octahedral positions. Such a structure is called normal spinel. If divalent cations A^{II} occupy the octahedral sites and B^{III} cations are distributed among tetrahedral and octahedral sites, the structure is called inverse spinel. Most of the ferrite properties depend on the cation distribution in the tetrahedral or octahedral sites in the spinel structure. The cation distribution is responsible of the number of vacancies and the non-stoichiometry, altering bulk and surface properties of the corresponding system, which is of special interest for catalysis [27]. These structural properties provide opportunities to extensively tune redox and electronic properties by varying the chemical composition of the ferrites to optimize their catalytic properties. It is noteworthy that in the spinel structure the octahedral sites are almost exclusively exposed at the surface of the solid and, therefore, the octahedral cations play a key role in determining the catalytic activity [28].

Spinel ferrites are transition metal oxide semiconductors and their oxidation or reduction can be evidenced by following the evolution of their electrical conductivity as a function of the nature of the gas phase in contact with the solid. Thus, exposure of a p-type semiconducting oxide to oxygen leads to the increase of its electrical conductivity with respect to that in inert atmosphere, according to the following equilibrium:

$$O_{2(gas)} \leftrightarrows O^{-}_{2(ads)} + h^{\bullet} \leftrightarrows 2O^{-}_{(ads)} + h^{\bullet} \leftrightarrows 2O^{2-}_{(ads)} + 2h^{\bullet} \leftrightarrows 2O^{\times}_{O} \qquad (1)$$

where $h^{\bullet}$ represents a hole and $O^{\times}_{O}$ a lattice oxygen anion of the solid. The electrons trapped by the adsorbed oxygen are provided by the valence band of the oxide where new positive holes are created. On the contrary, exposure to a reducing gas such as methane leads to the consumption of lattice oxygen with the subsequent formation of oxygen vacancies. In this case electrons are released in the valence band of the oxide resulting in the decrease of the positive holes concentration and thus in the decrease of the electrical conductivity.

In contrast with the p-type oxides, the exposure of a n-type semiconducting oxide to oxygen leads to the decrease of its electrical conductivity with respect to that in inert atmosphere, according to the equilibrium depicted in Eq. (2):

$$O_{2(gas)} + e' \leftrightarrows O^{-}_{2(ads)} + e' \leftrightarrows 2O^{-}_{(ads)} + 2e' \leftrightarrows 2O^{2-}_{(ads)} \leftrightarrows 2O^{\times}_{O} \qquad (2)$$

where e' represents a free electron. The electrons trapped by the adsorbed oxygen are in this case provided by the conduction band of the oxide and, consequently, the concentration of the charge carriers decreases. The exposure to a reducing gas such as methane leads to the consumption of lattice oxygen with the subsequent formation of oxygen vacancies but, in this case, electrons are released in the conduction band of the oxide resulting in the increase of the free electrons concentration and thus in the increase of the electrical conductivity.

It is well known that manganese and copper are key active components of the most active combustion catalysts based on transition metal oxides [29, 30]. On the other hand, among the ferrites studied as catalysts for VOC abatement, $CuFe_2O_4$ shows superior catalytic activities [19]. Moreover, Cu-containing mixed spinels were shown to be more active than $CuFe_2O_4$ simple spinel in CO oxidation [31]. Therefore, it was of interest to modify copper ferrite with manganese for obtaining $CuFe_{2-x}Mn_xO_4$ mixed spinels and to study their catalytic properties in the complete oxidation of methane as a VOC model compound. As these oxide materials are expected to be semiconductors functioning in the catalytic oxidation via a redox mechanism, it was also of interest to study their semiconductive and redox properties using *in situ* electrical conductivity measurements with the aim of explaining their catalytic behavior.

2. EXPERIMENTAL

2.1. Catalysts preparation and characterization

The $CuFe_{2-x}Mn_xO_4$ spinels were prepared by solid-state reactions between appropriate amounts of finely powdered oxides CuO 99.99 % (Aldrich), Fe_2O_3 99.98 % (Sigma-Aldrich) and Mn_2O_3 ≥ 99.99 % (Aldrich). The reactions were carried out in alumina boats under atmospheric air at 800 °C for 24 h. Such a high temperature is necessary for the complete formation of spinel phase [32].

Powder X-ray diffraction (XRD) patterns of the prepared spinels were recorded on a Philips diffractometer using Cu Kα radiation ($\lambda = 1.5418$ Å) at a scanning speed of $2° \min^{-1}$ in the 15-80° 2θ range.

Surface areas of the catalysts were measured from the adsorption isotherms of nitrogen at −196 °C using the BET method with a Micromeritics ASAP 2020 sorptometer. Before analysis the samples were outgassed at 200 °C overnight.

2.2. Catalytic measurements

The total oxidation of methane was carried out in a fixed bed quartz tube down-flow reactor operating at atmospheric pressure. The internal diameter of the reactor tube was 18 mm. 1 cm^3 (~ 1.5 g) of catalyst supported by quartz wool was always used. The axial temperature profile was measured using an electronic thermometer placed in a thermowell centered in the catalyst bed. Quartz chips were used to fill the dead volumes before and after the catalyst bed to minimize potential gas-phase reactions at high reaction temperatures. The reaction mixture consisted of 1 vol. % methane in air. The methane flow rate was controlled and measured using a Vögtlin Redy smart controller. The air flow rate was controlled by a fine needle valve and was measured by a capillary flow-meter. Steady-state catalytic measurements were performed at total gas hourly space velocity (GHSV) of 15000 h^{-1}, in the temperature range 450-800 °C.

Before each activity test, the reactor was heated to the desired temperature at a heating rate of 5 °C/min, and the reactant flows were set to give the desired reaction mixture. The system was allowed to stabilize for about 30 min at the reaction temperature before the first product analysis was made. Each run was carried out over a period of 1-2 hours, until two consecutive analyses were identical. The feed and the reactor outflow gases were analyzed on-line by a Clarus 500 Gas-Chromatograph equipped with a thermal conductivity detector (TCD), using two packed columns in series (6 ft Hayesep and 10 ft molecular sieve 5Å). After the catalytic test the reactor was cooled down under the flow of reactants.

The amount of raw material transformed in reaction divided by the amount that was fed to the reactor gave the conversion. Complete selectivity to CO_2 and H_2O was always observed. The carbon balance was satisfactory in all runs varying within the margin of error of ± 2 %.

2.3. Electrical conductivity measurements

The samples were compressed at ca. 2.76 x 10^7 Pa using a Carver 4350.L pellet press to ensure good electrical contacts between the catalyst grains. The obtained pellet was then placed in a horizontal quartz tube between two platinum electrodes. Flow rates of gases flowing over the sample were controlled by fine needle valves and were measured by capillary flow meters. The temperature was controlled using thermocouples soldered to the electrodes and, when by passed, they were used to determine the electrical conductivity σ of the samples, which can be expressed by the formula:

$$\sigma = \frac{1}{R} \times \frac{t}{S} \qquad (3)$$

where R is the electrical resistance and t/S is the geometrical factor of the pellet including the thickness t (ca. 3 mm) and the cross sectional area S of the pellet whose diameter was equal to 13 mm. The electrical resistance was measured with a megaohmmeter (FLUKE 177 Digital Multimeter).

To compare the electrical conductivities of the samples, it is required that the solids have similar textures and surface states. This requirement is easily fulfilled since all the samples have similar textures. Indeed, the electrical conductivity of semiconducting oxide powders can be written as:

$$\sigma = An \qquad (4)$$

where n is the concentration of the main charge carriers and A is a coefficient of proportionality which includes the mobility of the main charge carriers and the elementary charge of the electron and depends on the compression of the powder and on the number and quality of contact points between particles [33]. Since the samples were compressed at the same pressure and have similar BET surface areas and since the electrical measurements were standardized, A can be considered as identical for all the samples under identical conditions.

The common reference state for σ determination has been chosen under air at atmospheric pressure and at 640 °C. At this temperature, which is in the range used in the catalytic reactions, most of the ionically adsorbed species such as H_3O^+, HO^- which would produce an additional surface conductivity are eliminated. The solid was initially heated from room temperature to the desired temperature at a heating rate of 5 °C/min.

3. RESULTS AND DISCUSSION

3.1. Catalysts characterization

The XRD patterns of the $CuFe_{2-x}Mn_xO_4$ spinels are presented in Fig. 1. Obviously, all the samples showed a cubic spinel structure identified with PDFs 34-0425 and 71-1142 corresponding to $CuFe_2O_4$ and $CuMn_2O_4$ spinels, respectively. The well-defined sharp peaks indicate a good crystalline quality of the materials. Nevertheless, weak diffraction lines corresponding to CuO (PDF 80-1268) and α-Fe_2O_3 (PDF 33-0664) or α-Mn_2O_3 (PDF 73-1826) side phases were observed in all the samples. This means that the initial amounts of single oxides were incompletely consumed during the crystallization of spinel structure obviously due to the moderate temperature (800 °C) used for the solid state reaction. Based on Scherer's equation [34] the crystallite size was estimated to be in the range 42-74 nm (Table 1). This demonstrates that spinel phase with nanosized crystallites has been obtained.

As expected based on the method of preparation used, the specific surface areas of the $CuFe_{2-x}Mn_xO_4$ spinels (Table 1) were relatively low and comparable with those of similar spinels calcined at high temperatures [19]. The low surface areas observed suggests the agglomeration of the nanosized crystallites [19].

3.2. Catalytic properties

The $CuFe_{2-x}Mn_xO_4$ spinels with x = 0, 0.4, 0.8, 1.6 and 2, were tested in the total oxidation reaction of methane in the temperature range from 500 to 770 °C and 1 % vol. CH_4 in air (GHSV = 15000 h^{-1}). The methane conversions as a function of the reaction temperature were plotted in Fig. 1a. It can be observed that the ignition temperature was around 530 °C for all the catalysts and none of them gave a complete conversion of methane in the temperature range considered. $CuFe_2O_4$ was the most active, while $CuMn_2O_4$ was the least active in the series studied. The catalytic activity decreased with increasing the value of x in the $CuFe_{2-x}Mn_xO_4$ spinels as follows: $CuFe_2O_4 > CuFe_{1.6}Mn_{0.4}O_4 > CuFe_{1.2}Mn_{0.8}O_4 > CuFe_{0.4}Mn_{1.6}O_4 > CuMn_2O_4$. This order was confirmed by comparison of the temperatures corresponding to 10 % methane conversion (T_{10}) and of the specific reaction rates of the different catalysts measured at 710 °C presented in Table 2. Based on such comparisons, a detrimental effect of Mn incorporation in $CuFe_2O_4$ is observed.

The specific reaction rate was calculated according to Eq. (5)

$$r = k\frac{F_{CH_4,inlet}(1-x)}{Q_0} \tag{5}$$

where x is the degree of methane conversion at the reaction temperature T (K) considered, Q_0 the total flow rate (L s^{-1}), $F_{CH_4,inlet}$ the molar flow rate of methane at the inlet of the reactor (mol s^{-1}) and k the reaction rate constant (L g^{-1} s^{-1}).

It is well known that methane total oxidation follows a pseudo first order kinetics [5, 7, 35, 36] and the reaction rate constant can be calculated from the integrated equation of first order kinetics for the plug-flow reactor

$$k = \frac{Q_0}{W}\ln\frac{1}{1-x} \tag{6}$$

where W is the mass of catalyst (g). The apparent activation energies (E_a) on the $CuFe_{2-x}Mn_xO_4$ catalysts were calculated from the slope of the ln$k$ versus 1000/T plots shown in Fig. 1b. Only methane conversions lower than ca. 30 % were considered to avoid diffusion limitations. For all the catalysts studied a linear dependency was observed confirming the pseudo first order kinetics for the methane total oxidation over the catalysts studied. The apparent activation energies (E_a) on the different catalysts are reported in Table 2. They were in the range from 101.5 kJ mol^{-1} to 114.5 kJ mol^{-1}. The lowest value calculated for $CuFe_2O_4$ can explain its highest catalytic activity.

The introduction of Mn in the $CuFe_2O_4$ structure increases the apparent activation energy, then it decreases with increasing the value of x in $CuFe_{2-x}Mn_xO_4$ spinels. At the same time, a compensation effect is observed as the pre-exponential factor decreases following the same way (Table 2) probably due to a decrease in the density of active sites with increasing Mn content. This effect explains the decrease of the specific activity with increasing the Mn content.

3.3. Electrical conductivity measurements

a) Variations of the electrical conductivity as a function of temperature

The electrical conductivities of the ferrite samples have been measured as a function of temperature to determine the activation energy of conduction E_c, both under air and under nitrogen at atmospheric pressure, in the temperature range from 400 to 760 °C. The semi-log plots [$\log\sigma = f(1/T)$] obtained are given in Fig. 3. The linear variations observed showed that all the solids behaved as semiconductors both under air and under nitrogen and their electrical conductivities varied exponentially with temperature. The slopes of the semi-log plots enabled one to calculate the E_c values presented in Table 1. It can be observed that the E_c values under nitrogen were lower than under air for all the oxides but varied similarly, as follows: they increased by substituting Mn to Fe in $CuFe_2O_4$ and by increasing its content in ternary spinels $CuFe_{2-x}Mn_xO_4$ up to x = 1.6, then decreased for $CuMn_2O_4$. This behavior can be attributed to the modification of the nature of the energy band structure, as well as to the shift of the energy level impurities into the forbidden band gap with increasing Mn content in ternary spinels. It is noteworthy that the activation energies of the $CuFe_2O_4$ and $CuMn_2O_4$ samples under air are comparable with the values reported in the literature [37, 38].

The electrical conductivities of the catalysts under air and under nitrogen were compared in Fig. 3 for determining the nature of the semiconductor type of the solid by applying the Heckelsberg criterion [39]. According to this criterion, if the conductivity of an oxide is higher under oxygen (air) than under an inert gas, i.e. nitrogen, then it is a p-type semiconductor. In contrast, if the conductivity of an oxide is lower under air than under nitrogen, then it is a n-type semiconductor. This is due to fact that the electrons trapped by the adsorbed oxygen, which always adsorbs as anionic species, are provided by the valence band of the oxide in the case of a p-type semiconductor or by its conduction band in the case of a n-type semiconductor. In the first case new positive holes are created and, thus, the electrical conductivity increases while in the second case the concentration of charge carriers (free electrons) is diminished and the electrical conductivity decreases. As it can be seen in Fig. 3, the electrical conductivity was higher in air flow than in nitrogen flow for $CuFe_2O_4$ and lower for $CuMn_2O_4$ within all the temperature range considered. This clearly suggests that, according to the Heckelsberg criterion, the first compound is a p-type semiconductor and the second one a n-type semiconductor. For the $CuFe_{2-x}Mn_xO_4$ samples, with x = 0.4, 0.8 and 1.6, the electrical conductivity in air flow was higher than in nitrogen flow at high temperatures and lower at low temperatures. This suggests that both types of conduction mechanisms are present in the ternary spinels, being predominant one or another as a function of temperature. Thus, at low temperatures they behave as n-type semiconductors while at high temperatures as p-type. The change from one type of semiconducting behavior to another was observed at 540, 520 and 480 °C for $CuFe_{1.6}Mn_{0.4}O_4$, $CuFe_{1.2}Mn_{0.8}O_4$ and $CuFe_{0.4}Mn_{1.6}O_4$, respectively. This change took place at temperatures lower or around the ignition temperature of the catalysts, i.e. 530 °C, and therefore all the ternary spinels were of p-type in the reaction temperature range.

Note that the existence of both n- and p-type conduction mechanisms was already observed for $CuFe_2O_4$ [37], the two competing mechanisms being associated to the following reactions:

$$Fe^{2+} \leftrightarrows Fe^{3+} + e' \tag{7}$$

$$Cu^{2+} \leftrightarrows Cu^{+} + h^{\bullet} \tag{8}$$

where e' stands for electrons and $h^{\bullet}$ for holes. The type of charge carriers and their concentration are determined by the kinetics of the reactions (7) and (8) [37].

b) Variations of the electrical conductivity under air as a function of oxygen partial pressure

Fig. 4 shows the variations of σ as a function of oxygen pressure at 640 °C in a log–log plot for the $CuFe_{2-x}Mn_xO_4$ samples with x = 0, 0.8 and 2. It clearly appeared that no dependence of σ on the oxygen pressure was observed for all the samples. This would rather agree with the fact that these materials are intrinsic semiconductors ($\partial\sigma/\partial P_{O_2} = 0$). If that was true, the theory would imply that the band-gap energy E_G should be equal to twice the activation energy of conduction E_c ($E_G = 2E_c$). The UV spectra of the samples presented in Fig. 5 were used to determine their band-gap energies. Indeed, the band-gap energies were obtained from the plots $(\alpha h\nu)^2$ vs. $h\nu$ by extrapolating the straight line which intercept the energy axes $h\nu$ (Fig. S1). The absorption coefficient α, which depend on the wavelength, is proportional to $\ln[(R_{max} - R_{min})/(R - R_{min})]$, where the reflectance decreased from R_{max} to R_{min} due to the semiconductor absorption and R is the intermediate for any intermediate energy photons [40]. Table 1 shows the band-gap energies obtained. It can be observed that the band-gap energies determined from the UV spectra were different from those calculated. Consequently, the solids cannot be considered intrinsic but extrinsic semiconductors under our conditions with sources of electrical charge carriers independent of oxygen pressure.

c) ***In situ*** **electrical conductivity measurements under catalytic conditions.**

To get information on the solids under conditions as close as possible to those of catalysis, the electrical conductivity of the $CuFe_{2-x}Mn_xO_4$ samples with x = 0, 0.8 and 2 was measured at 640 °C, i.e. within the reaction temperature range, during sequential periods under air, under methane-air mixture (reaction mixture) and under methane-nitrogen mixture (Fig. 6). The solids were heated from room temperature to 640 °C, at a heating rate of 5 °C min^{-1} in air flow at atmospheric pressure. After reaching the steady state under the air flow, a methane-air mixture was passed over the samples. For the samples with x = 0 and 0.8 the electrical conductivity slightly increased while for the sample with x = 2 it slightly decreased. The behavior of the samples with x = 0 and 0.8 corresponds to the n-type semi-conducting character since, for oxide semiconductors, the n-type criterion is $\partial\sigma/\partial P_{O_2} < 0$ or, considering methane as a reductant, $\partial\sigma/\partial P_{CH_4} > 0$, while that of the sample with x = 2 corresponds to the p-type semi-conducting character since the p-type criterion is $\partial\sigma/\partial P_{O_2} > 0$ or $\partial\sigma/\partial P_{CH_4} < 0$. After reaching the steady state under the methane-air flow, the atmosphere was again switched to air. The electrical conductivity decreased and reached a plateau for the $CuFe_{2-x}Mn_xO_4$ samples with x = 0 and 0.8 confirming their n-type semi-conducting character, while for the $CuMn_2O_4$ sample (x = 2) it increased confirming its p-type character. After reaching again the steady state under air flow, the atmosphere was switched to a methane-nitrogen mixture before the air sequence was repeated for testing the reversibility of the phenomena. Again, an important increase of the electric conductivity was observed for the $CuFe_{2-x}Mn_xO_4$ samples with x = 0 and 0.8 corresponding to their n-type semi-conducting character. Under air their electrical conductivities decreased immediately and reached a plateau confirming the reversibility of the phenomena observed. However, for the ternary spinel sample (x = 0.8) the reversibility was not complete as the plateau corresponding to the new steady state under air was not the same as before the methane-nitrogen mixture sequence, suggesting a new state of the solid that obviously corresponds to a reduced oxide. For the $CuMn_2O_4$ sample (x = 2), the electrical conductivity decreased under the methane-nitrogen flow suggesting again a p-type character for this sample. Under air, its electrical conductivity increased and reached a plateau identical to that reached before reduction suggesting a completely reversible reduction of the solid.

It is interesting to note that the introduction of methane in the flow in contact with the solid changed the nature of the semiconductivity of all the solids. The $CuFe_{2-x}Mn_xO_4$ samples with x = 0 and 0.8 passed from p-type in air (Fig. 3) to n-type conduction, while $CuMn_2O_4$ passed from n-type in air (Fig. 3) to p-type conduction. This change from p-type in air to n-type in the presence of a hydrocarbon was already observed for Ti and Zr pyrophosphates [41].

The reversible redox process observed in the case of the $CuFe_{2-x}Mn_xO_4$ samples with x = 0 and 0.8 during successive sequences under methane-air mixture or methane-nitrogen mixture and pure air can be explained by the oxidation of methane by lattice oxygen anions on the catalyst surface, which leads to a partially reduced surface as already suggested for the oxidative dehydrogenation of *n*-butane over metal pyrophosphates [41, 42] and for propane ammoxidation over VAlO mixed oxides [43]. Thus, the increase of σ can be ascribed to the creation of anionic vacancies:

$$O_O^\times + CH_4 \rightarrow \text{Oxidation products} + V_O^\times \qquad (9)$$

followed by their spontaneous ionization:

$$V_O^\times \rightleftarrows V_O^\bullet + e' \qquad (10)$$

$$V_O^\bullet \rightleftarrows V_O^{\bullet\bullet} + e' \qquad (11)$$

where $O_O^\times$ represents an oxygen anion of the solid in regular lattice points (O^{2-}), $V_O^\times$ a filled anionic vacancy, $V_O^\bullet$ a singly ionized anionic vacancy and $V_O^{\bullet\bullet}$ a doubly ionized anionic vacancy. The release of free electrons into the conduction band of the solid accounts for the observed increase in electrical conductivity. The subsequent introduction of air over the samples restores the initial value of σ indicating the refilling of the previously created anionic vacancies by dissociation of oxygen and capture of free electrons:

$$1/2O_2 + V_O^\bullet + e' \rightleftarrows O_O^\times \qquad (12)$$

$$1/2O_2 + V_O^{\bullet\bullet} + 2e' \leftrightarrows O_O^{\times} \tag{13}$$

This behavior is in agreement with a Mars – van Krevelen type mechanism [44].

The case of $CuMn_2O_4$ sample (x = 2) is different as it behaves as a p-type semiconductor with holes, $h^{\bullet}$, as the main charge carriers under the reaction conditions. If one considers that from the chemical point of view, a positive hole corresponds to an electron vacancy in the valence band of lattice $O_O^{\times}$ anions, i. e. the "chemical site" of a positive hole corresponds in fact to a lattice $O_O^{\bullet}$ anion [45, 46], according to the reaction:

$$O_O^{\times} + h^{\bullet} \leftrightarrows O_O^{\bullet} \tag{14}$$

the initial activation step of methane over $CuMn_2O_4$ catalyst can be written:

$$CH_4 + O_O^{\bullet} \rightarrow CH_3^{\bullet} + (HO^-)^{\bullet} \tag{15}$$

as already suggested for titanate-based catalysts [47] and $LaCo_{1-x}Fe_xO_3$ perovskites [48].

Water elimination generates oxygen vacancies, according to the reaction:

$$2(HO^-)^{\bullet} \leftrightarrows H_2O_{(g)} + O_O^{\times} + V_O^{\bullet\bullet} \tag{16}$$

Carbon dioxide formation also involves positive holes consumption and generates oxygen vacancies, according to the simplified reactions:

$$C + 2\,O_O^{\bullet} + 2\,h^{\bullet} \leftrightarrows CO_{2(g)} + 2\ V_O^{\bullet\bullet} \tag{17}$$

or

$$C + 2\,O_O^{\times} + 4\,h^{\bullet} \leftrightarrows CO_{2(g)} + 2\ V_O^{\bullet\bullet} \tag{18}$$

where, for simplicity, we considered a carbon atom, C, instead of CH_x species. The formation of oxygen vacancies is in line with the observed reduction of the solid under methane-air and methane-nitrogen flows. These vacancies must be filled in by gaseous oxygen in order to reoxidize the solid:

$$1/2O_{2(g)} + V_O^{\bullet\bullet} \rightarrow O_O^{\times} + 2\,h^{\bullet} \tag{19}$$

This suggests that the overall reaction mechanism over the $CuMn_2O_4$ catalyst can also be assimilated to a Mars – van Krevelen type mechanism [44], but in this case the methane transformation involves mainly surface lattice O^- species ($O_O^{\bullet}$), whereas for the other $CuFe_{2-x}Mn_xO_4$ catalysts, surface lattice O^{2-} anions ($O_O^{\times}$) are mainly involved. Nevertheless, as the $CuFe_{2-x}Mn_xO_4$ catalysts with x = 0, 0.4, 0.8 and 1.6 behave as p-type semiconductors under air, the initial activation step of methane involving O^{-} species according to Eq. (15) cannot be excluded.

It is interesting to note that as the O^{-} species are known to be quite active species for alkanes' oxidation [45], a high activity would be expected for the $CuMn_2O_4$ catalyst. The weak variations of the electrical conductivity observed in that case (Fig. 6) suggest a low concentration of O^{-} species on the catalyst surface explaining its low catalytic activity.

Finally, we note that no direct correlations between the catalytic reaction and conduction parameters of the studied ferrites were observed. This may be due to the complex nature of their electrical behavior, which changes from a conduction type to another both as a function of temperature and of the nature of the gas phase in contact with the solid.

4. CONCLUSION

Nanosized cubic spinels with $CuFe_{2-x}Mn_xO_4$ composition (x = 0, 0.4, 0.8, 1.6 and 2) have been prepared by solid-state reactions between the corresponding oxides. Their catalytic activity in the total oxidation of methane in the temperature range from 500 to 800 °C, decreased with increasing the Mn content, i.e. the value of x, as follows: $CuFe_2O_4$ > $CuFe_{1.6}Mn_{0.4}O_4$ > $CuFe_{1.2}Mn_{0.8}O_4$ > $CuFe_{0.4}Mn_{1.6}O_4$ > $CuMn_2O_4$. None of the catalysts gave complete conversion of methane in the temperature range chosen. A pseudo first order kinetics of the methane total oxidation reaction was noted for all the catalysts. $CuFe_2O_4$ appeared to be a p-type semiconductor while $CuMn_2O_4$ a n-type semiconductor under air in the reaction temperature range but $CuFe_2O_4$ became n-type while $CuMn_2O_4$ p-type when contacted with methane. Both types of conduction mechanisms are present in $CuFe_{2-x}Mn_xO_4$ spinels with x = 0.4, 0.8 and 1.6, being predominant one or another as a function of temperature. Nevertheless, they were of p-type under air in the reaction temperature range and became of n-type when contacted with methane. *In situ* changes in the electrical conductivity under different gaseous atmospheres showed that all the catalysts are partially reduced during catalysis and provide clear and direct evidence for a redox mechanism with consumption of surface lattice oxygen. It can be assimilated to a Mars and van Krevelen mechanism involving mainly surface lattice O^{-} species for $CuMn_2O_4$ catalyst and surface lattice O^{2-} anions for all other catalysts studied.

ACKNOWLEDGMENTS

Ionel Popescu expresses his gratitude to the management staff of the University of Bucharest, especially to the Vice Rector Prof. Emil Barna, for the financial support within the frame of the project UB 256/2014.

REFERENCES

1. M.R. Morales, B.P. Barbero, L.E. Cadús, Appl. Catal. B 67 (2006) 229-236.
2. R.M. Heck, R.J. Farrauto, Catalytic Air Pollution Control. Commercial Technology, Van Nostrand Reinhold, New York, 1995.
3. R. Craciun, B. Nentwich, K. Hadjiivanou, H. Knozinger, Appl. Catal. A 243 (2003) 67-79.
4. T. Machej, E.M. Serwicka, M. Zimowska, R. Dula, A. Michalik-Zym, B. Napruszewska, W. Rojek, R. Socha, Appl. Catal. A 474 (2014) 87-94.
5. M. Răciulete, G. Layrac, D. Tichit, I.C. Marcu, Appl. Catal. A 477 (2014) 195-204.
6. N. T. Binh, C. Gennequin, R. Cousin, E. A. Zhilinskaya, H. L. Tidahy, N. M. Son, V. T. Thu Ha, L. T. Son, N. T. Minh Thu, P. X. Nui, S. Siffert, Chimica Oggi / Chemistry Today 31 (2013) 51-54.
7. A. Urdă, I. Popescu, T. Cacciaguerra, N. Tanchoux, D. Tichit, I.C. Marcu, Appl. Catal. A 464-465 (2013) 20-27.
8. J. Ludvíková, K. Jirátová, J. Klempa, V. Boehmová, L. Obalová, Catal. Today 179 (2012) 164- 169.
9. A. Kaddouri, N. Dupont, P. Gélin, P. Delichère, Catal. Lett. 141 (2011) 1581-1589.
10. S. Tanasoi, G. Mitran, N. Tanchoux, T. Cacciaguerra, F. Fajula, I. Săndulescu, D. Tichit, I.C. Marcu, Appl. Catal. A 395 (2011) 78-86.
11. F. Kovanda, K. Jirátová, Appl. Clay Sci. 53 (2011) 305-316.
12. R. Dziembaj, M. Molenda, L. Chmielarz, M. Drozdek, M. M. Zaitz, B. Dudek, A. Rafalska-Łasocha, Z. Piwowarska, Catal. Lett. 135 (2010) 68-75.
13. A. Urdă, I. Popescu, I.C. Marcu, G. Cârjă, N. Apostolescu, I. Săndulescu, Rev. Chim. 61 (2010) 267-271.
14. S. Rousseau, S. Loridant, P. Delichère, A. Boreave, J.P. Deloume, P. Vernoux, Appl. Catal. B 88 (2009) 438-447.
15. I. Popescu, A. Urda, T. Yuzhakova, I.C. Marcu, J. Kovacs, I. Săndulescu, C. R. Chim. 12 (2009) 1072-1078.

16. Y. Li, Y. Guo, B. Xue, Fuel Proc. Technol. 90 (2009) 652-656.
17. S. Tanasoi, N. Tanchoux, A. Urdă, D. Tichit, I. Săndulescu, F. Fajula, I.C. Marcu, Appl. Catal. A 363 (2009) 135-142.
18. N. Rezlescu, E. Rezlescu, P.D. Popa, C. Doroftei, M. Ignat, Appl. Catal. B 158-159 (2014) 70-75.
19. N. Rezlescu, E. Rezlescu, P.D. Popa, E. Popovici, C. Doroftei, M. Ignat, Mater. Chem. Phys. 137 (2013) 922-927.
20. C. Munteanu, M. Caldararu, D. Gingasu, M. Feder, L. Diamandescu, N. I. Ionescu, Reac. Kinet. Mech. Catal. 104 (2011) 357-368.
21. T. Tsoncheva, E. Manova, N. Velinov, D. Paneva, M. Popova, B. Kunev, K. Tenchev, I. Mitov, Catal. Commun. 12 (2010) 105-109.
22. M. Florea, M. Alifanti, V.I. Parvulescu, D. Mihaila-Tarabasanu, L. Diamandescu, M. Feder, C. Negrila, L. Frunza, Catal. Today 141 (2009) 361-366.
23. A. Urdă, A. Herraïz, Á. Rédey, I.C. Marcu, Catal. Commun. 10 (2009) 1651-1655.
24. J.E. Tasca, C.E. Quincoces, A. Lavat, A.M. Alvarez, M.G. González, Ceram. Int. 37 (2011) 803-812.
25. J.B. Silva, C.F. Diniz, R.M. Lago, N.D.S. Mohallem, J. Non-Cryst. Solids 348 (2004) 201-204.
26. A. Goldman, Modern Ferrite Technology, 2nd ed., Springer, Pittsburg, 2006.
27. J.A. Toledo-Antonio, N. Nava, M. Martínez, X. Bokhimi, Appl. Catal. A 234 (2002) 137-144.
28. J.P. Iacobs, A. Maltha, J. Drimal, V. Ponec, H.H. Brongersma, J. Catal. 47 (1994) 294-300.
29. T.V. Choudhary, S. Banerjee, V.R. Choudhary, Appl. Catal. A 234 (2002) 1-23.
30. W.B. Li, J.X. Wang, H. Gong Catal. Today 148 (2009) 81-87.
31. C.U. Aniz, T.D.R. Nair, Open J. Phys. Chem. 1 (2011) 124-130.
32. K. Faungnawakij, Y. Tanaka, N. Shimoda, T. Fukunaga, S. Kawashima, R. Kikuchi, K. Eguchi, Appl. Catal. A 304 (2006) 40-48.
33. J.-M. Herrmann, in: *Catalyst Characterization, Physical Techniques for Solid Materials*, B. Imelik and J. C. Védrine (eds.), Plenum Press, New York, 1994, ch. 20.
34. H. Klung, L. Alexander, X-ray Diffraction Procedures, Wiley, New York, 1962.

35. Z. Jiang, J. Yu, J. Cheng, T. Xiao, M.O. Jones, Z. Hao, P. P. Edwards, Fuel Proc. Technol. 91 (2010) 97-102.
36. S. Pengpanich, V. Meeyoo, T. Rirksomboon, K. Bunyakiat, Appl. Catal. A 234 (2002) 221-233.
37. R.K. Selvan, C.O. Augustin, L.J. Berchmans, R. Saraswathi, Mat. Res. Bull. 38 (2003) 41-54.
38. D.B. Ghare, A.P.B. Sinha, L. Singh, J. Mater. Sci. 3 (1968) 389-394.
39. L. F. Heckelsberg, A. Clark, G. C. Bailey, J. Phys. Chem. 60 (1956) 559-561.
40. V. Kumar, T.P. Sharma, J. Phys. Chem. Solids 59 (1998) 1321-1325.
41. I.C. Marcu, J.M.M. Millet, J.M. Herrmann, Catal. Lett. 78 (2002) 273-279.
42. I.C. Marcu, I. Săndulescu, Y. Schuurman, J.M.M. Millet, Appl. Catal. A 334 (2008) 207-216.
43. J. Bilde, C. Janke, C. Lorentz, P. Delichere, I. Popescu, I.C. Marcu, S. Loridant, A. Brückner, J.M.M. Millet, J. Phys. Chem. C 117 (2013) 22926-22938.
44. S. Mars, N. van Krevelen, Chem. Eng. Sci., Special Sup. 9 (1954) 41-57.
45. J.M. Herrmann, P. Vernoux, K.E. Béré, M. Abon, J. Catal. 167 (1997) 106-117.
46. J.M.M. Millet, Top. Catal. 38 (2006) 83-92.
47. I. Popescu, I. Săndulescu, Á. Rédey, I.C. Marcu, Catal. Lett. 141 (2011) 445-451.
48. I. Popescu, Y. Wu, P. Granger, I.C. Marcu, Appl. Catal. A 485 (2014) 20-27.

FIGURES CAPTION

Figure 1. XRD patterns of the $CuFe_{2-x}Mn_xO_4$ spinels: (a) $CuFe_2O_4$; (b) $CuFe_{1.6}Mn_{0.4}O_4$; (c) $CuFe_{1.2}Mn_{0.8}O_4$; (d) $CuFe_{0.4}Mn_{1.6}O_4$; (e) $CuMn_2O_4$. Symbols: ▼ – cubic ferrite; ■ – α-Fe_2O_3; # – α-Mn_2O_3; ● – CuO.

Figure 2. The light-off curves (a) and the corresponding Arrhenius plots (b) for the combustion of methane over the spinel catalysts (reaction conditions: GHSV = 15000 h^{-1}, 1 vol. % CH_4 in air): ■ – $CuFe_2O_4$; ◆ – $CuFe_{1.6}Mn_{0.4}O_4$; ● – $CuFe_{1.2}Mn_{0.8}O_4$; ∗ – $CuFe_{0.4}Mn_{1.6}O_4$; ▲ – $CuMn_2O_4$.

Figure 3. Arrhenius plots for the electrical conductivity σ of $CuFe_2O_4$ (a), $CuFe_{1.6}Mn_{0.4}O_4$ (b), $CuFe_{1.2}Mn_{0.8}O_4$ (c), $CuFe_{0.4}Mn_{1.6}O_4$ (d) and $CuMn_2O_4$ (e) under air (∗ and filled symbols) and under nitrogen (+ and open symbols) (σ in ohm^{-1} cm^{-1}).

Figure 4. Variation of σ as function of the oxygen pressure for $CuFe_2O_4$ (■), $CuFe_{1.2}Mn_{0.8}O_4$ (●) and $CuMn_2O_4$ (▲) at 640°C (P_{O_2} in atm; σ in ohm^{-1} cm^{-1}).

Figure 5. UV-VIS spectra of the $CuFe_{2-x}Mn_xO_4$ spinels: (a) $CuFe_2O_4$; (b) $CuFe_{1.6}Mn_{0.4}O_4$; (c) $CuFe_{1.2}Mn_{0.8}O_4$; (d) $CuFe_{0.4}Mn_{1.6}O_4$; (e) $CuMn_2O_4$.

Figure 6. Variation of the electrical conductivity under sequential exposures to air, methane – air mixture (reaction mixture) and methane – nitrogen mixture for $CuFe_2O_4$ (■), $CuFe_{1.2}Mn_{0.8}O_4$ (●) and $CuMn_2O_4$ (▲) at 640°C (σ in ohm^{-1} cm^{-1}).

Table 1. Physico-chemical characteristics of the $CuFe_{2-x}Mn_xO_4$ spinels.

Catalyst	SSA [a] (m^2 g^{-1})	D [b] (nm)	E_c [c] (kJ mol^{-1})		Theoretical E_G [d] (eV)	Experimental E_G [d] (eV)
			in air	in N_2		
$CuFe_2O_4$	2.2	74	54.8	51.2	1.14	1.86
$CuFe_{1.6}Mn_{0.4}O_4$	3.4	42	69.8	54.4	1.44	1.81
$CuFe_{1.2}Mn_{0.8}O_4$	2.6	47	71.4	59.4	1.48	1.80
$CuFe_{0.4}Mn_{1.6}O_4$	2.5	43	77.3	70.0	1.60	1.66
$CuMn_2O_4$	5.5	58	67.1	52.5	1.40	1.78

[a] Specific surface area.
[b] Average crystallite size.
[c] Activation energy of conduction in the temperature range 400-760°C.
[d] Band-gap energy.

Table 2. Catalytic performances in methane total oxidation of the $CuFe_{2-x}Mn_xO_4$ spinel catalysts.

Catalyst	T_{10} (°C)	Reaction rate at 710 °C		lnk_0 (k_0 in L g^{-1} s^{-1})	E_a (kJ mol^{-1})
		Specific (×10^{-7} mol g^{-1} s^{-1})	Intrinsic (×10^{-7} mol m^{-2} s^{-1})		
$CuFe_2O_4$	637	2.7	1.2	5.3	101.5
$CuFe_{1.6}Mn_{0.4}O_4$	667	2.1	0.6	6.5	114.5
$CuFe_{1.2}Mn_{0.8}O_4$	667	1.9	0.7	6.1	111.2
$CuFe_{0.4}Mn_{1.6}O_4$	673	1.8	0.7	5.5	106.8
$CuMn_2O_4$	680	1.6	0.3	5.1	104.2

Figure 1.

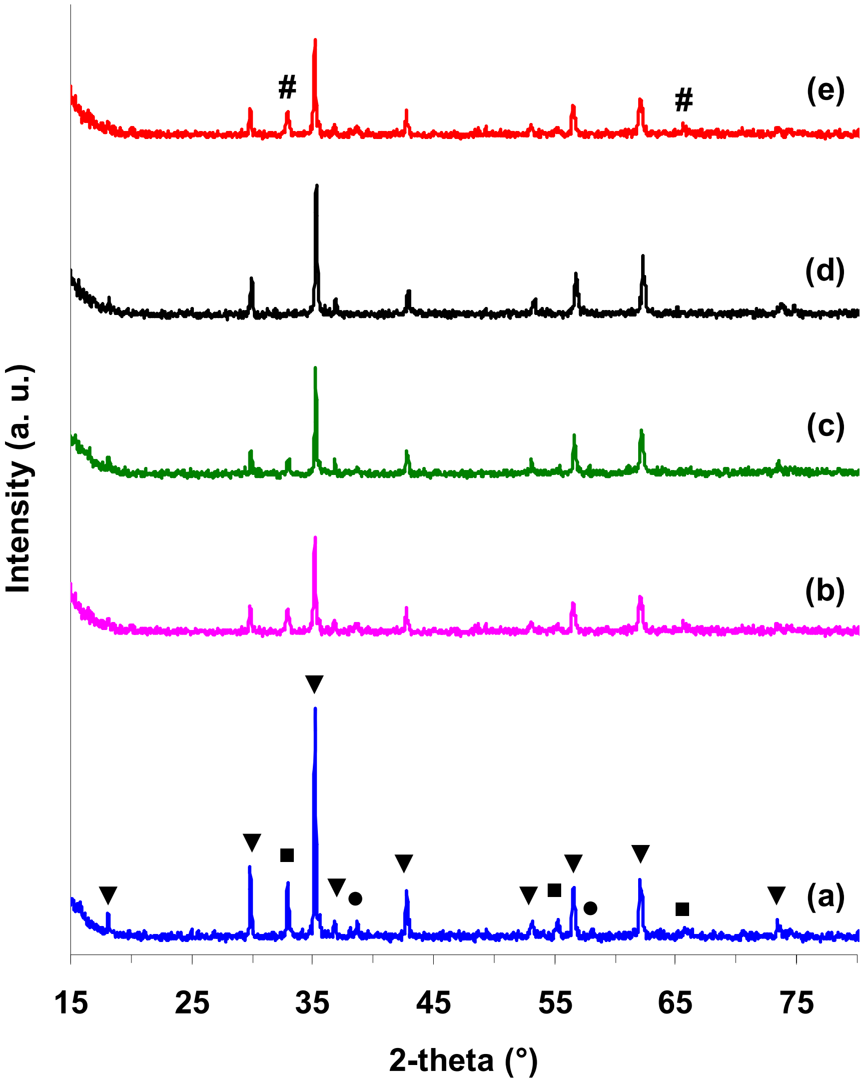

Figure 2.

(a)

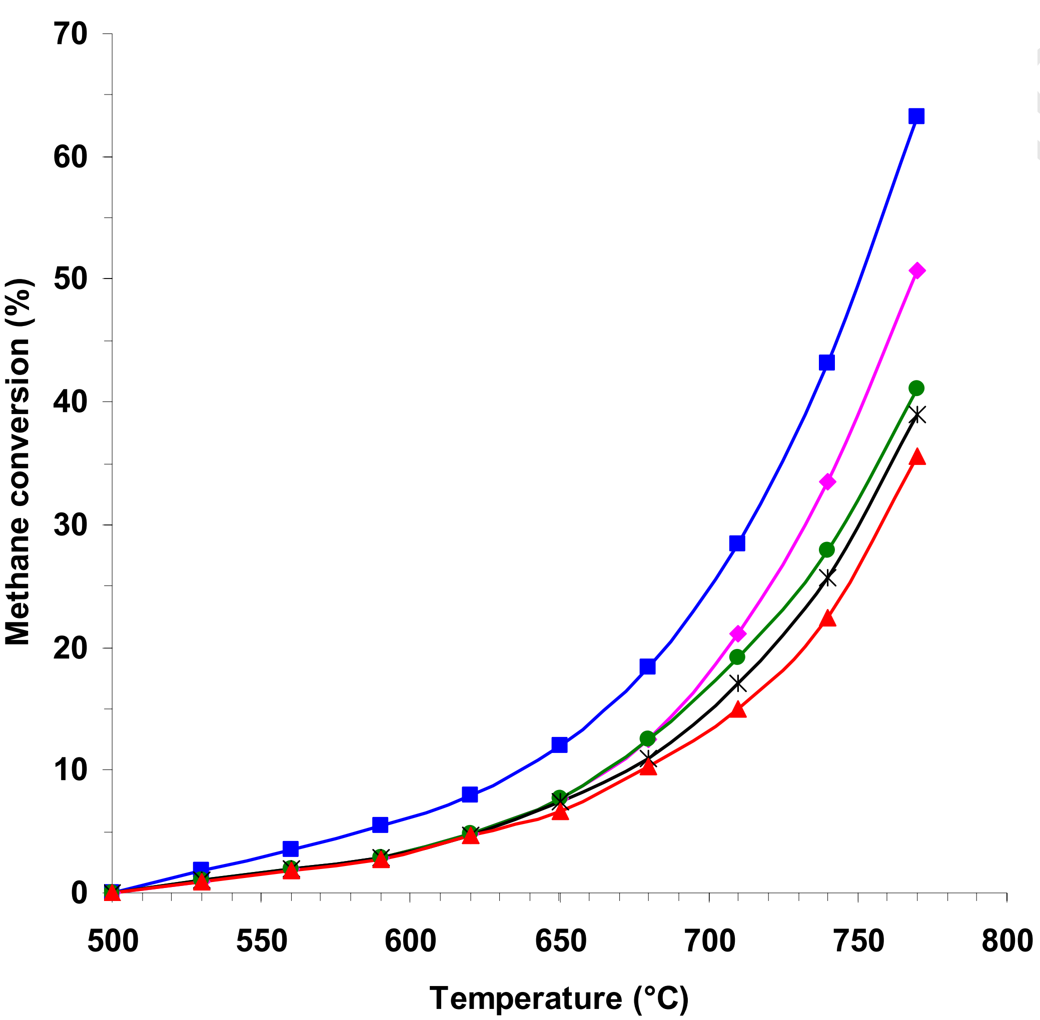
70
60
50
40
30
20
10
0
Methane conversion (%)
500
550
600
650
700
750
800
Temperature (°C)

(b)

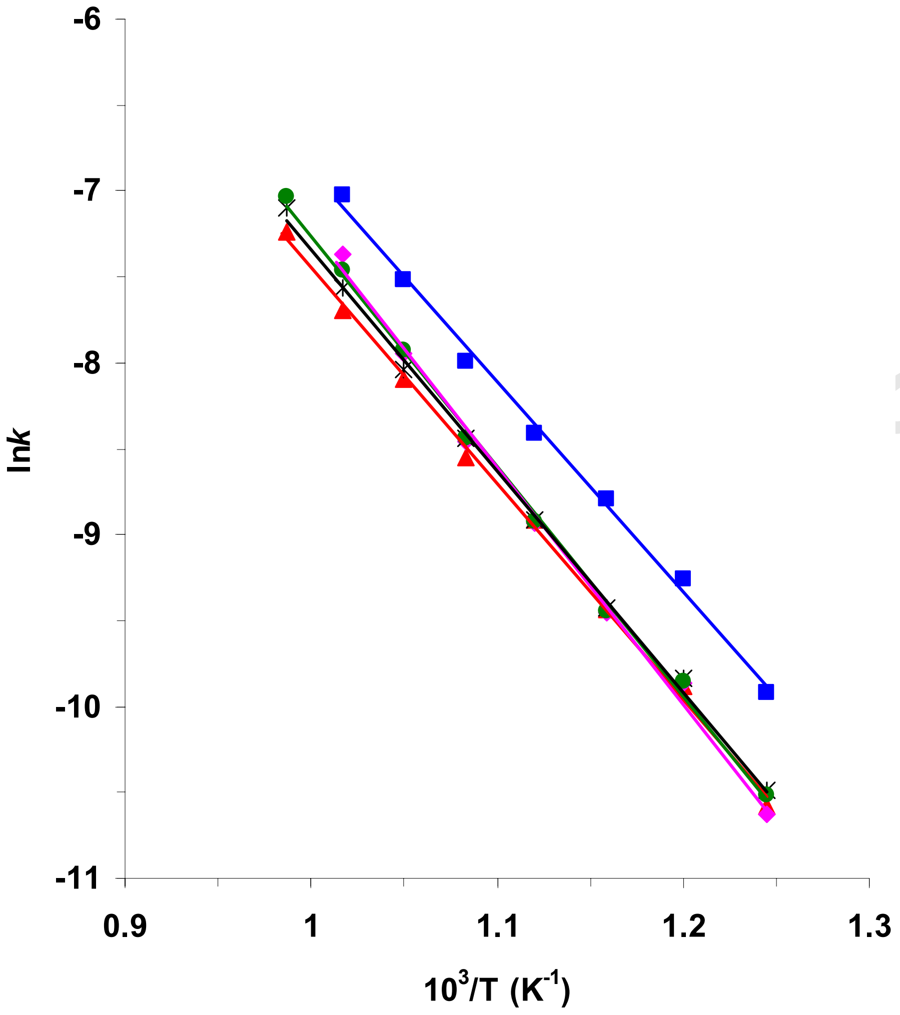

Figure 3.

(a)

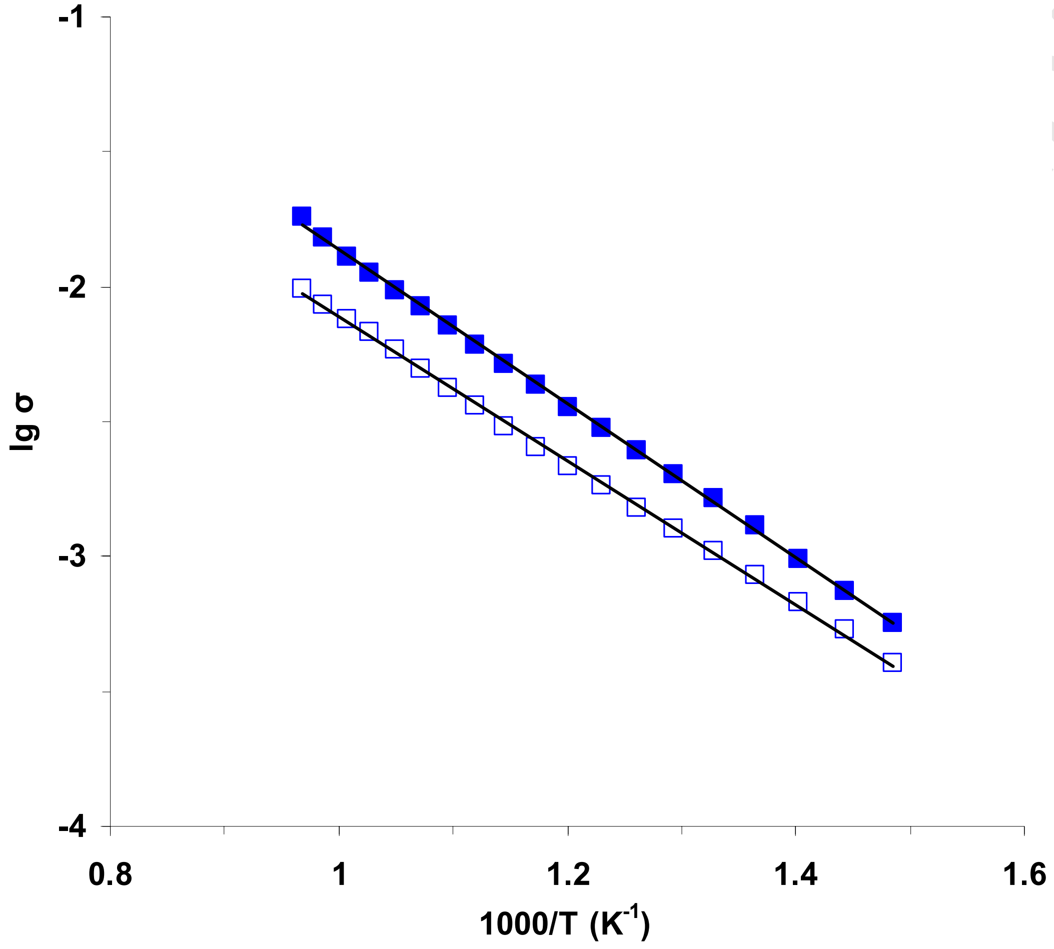

(b)

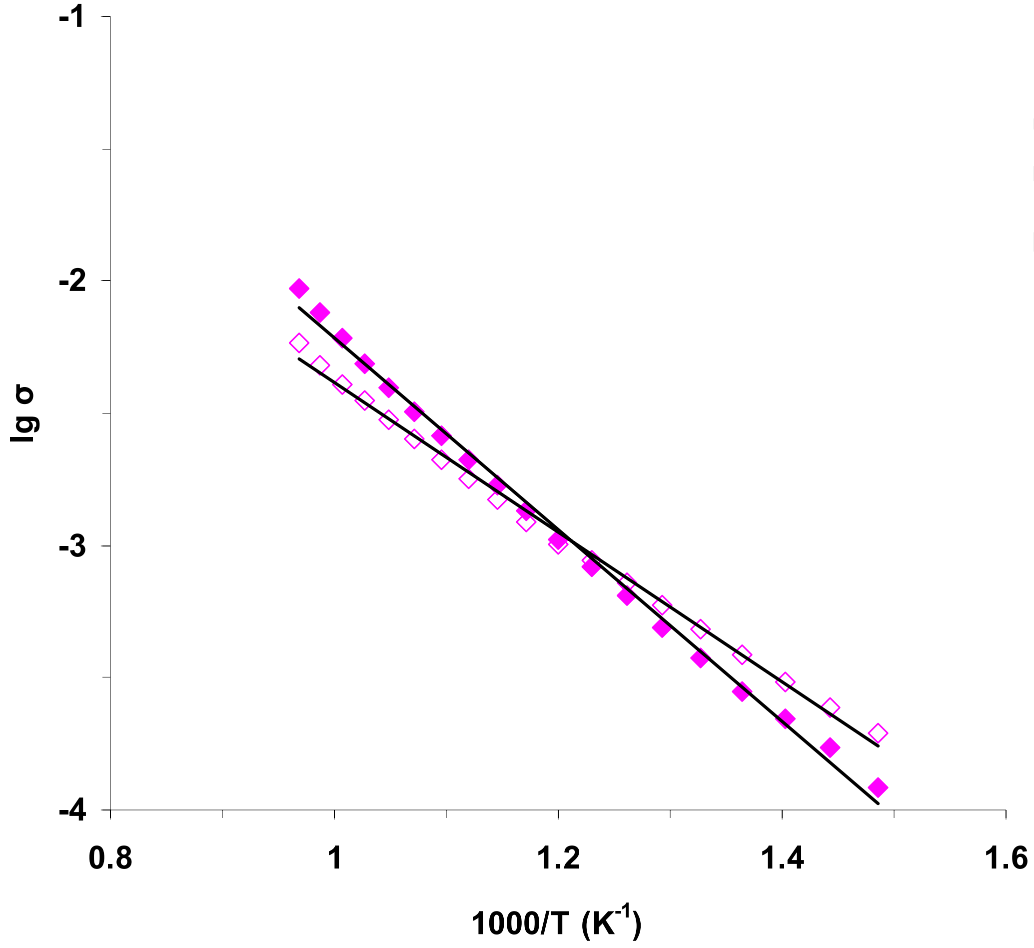

(c)

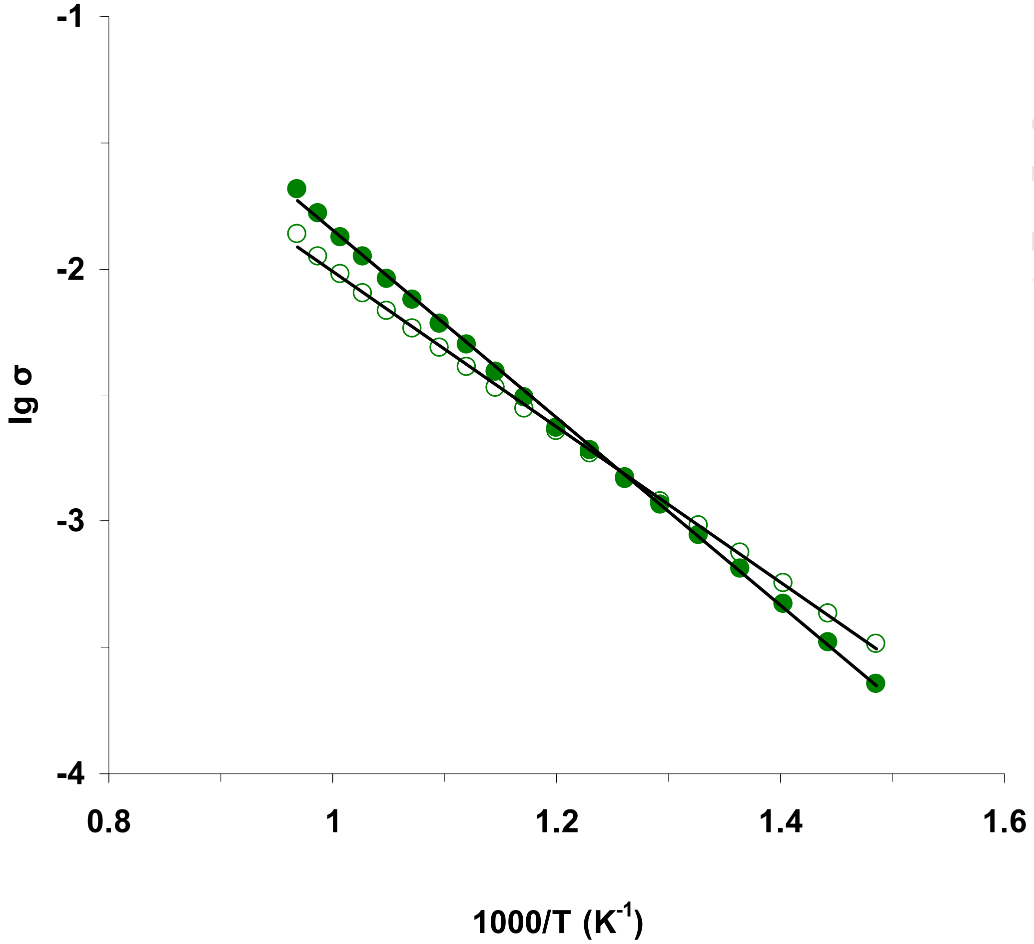

(d)

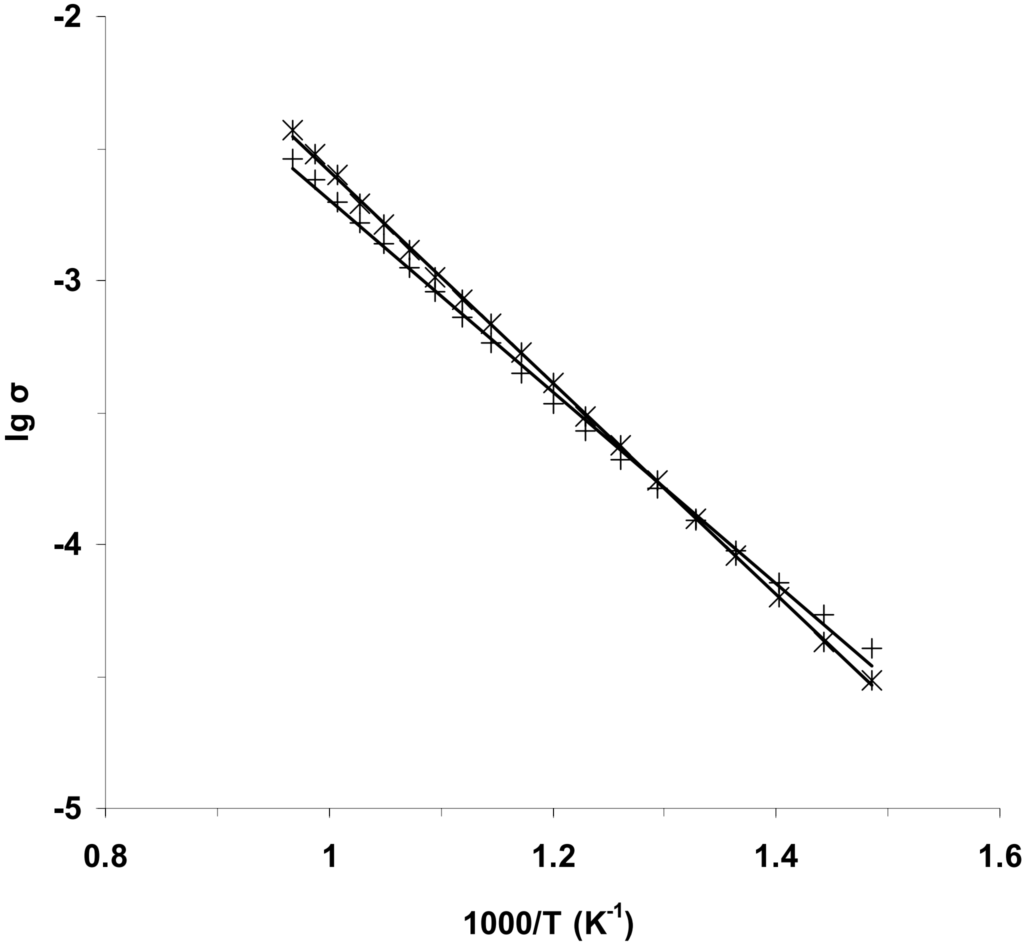

(e)

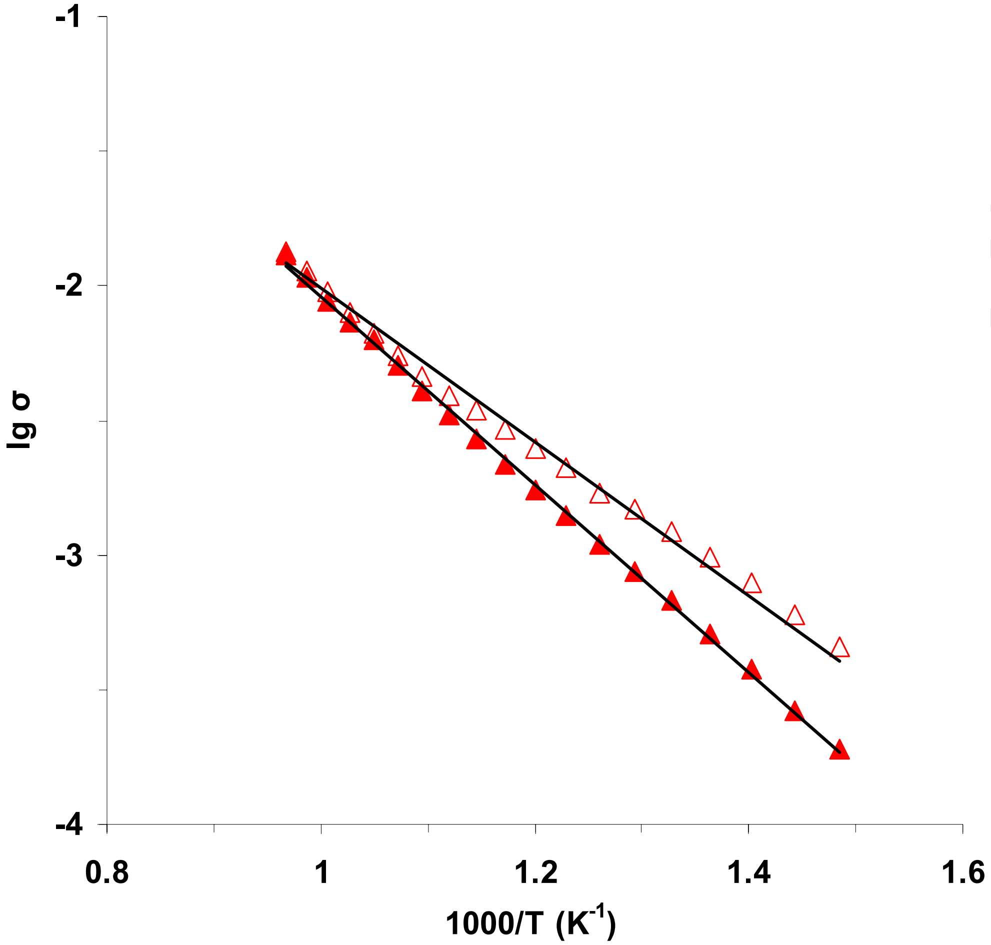

Figure 4.

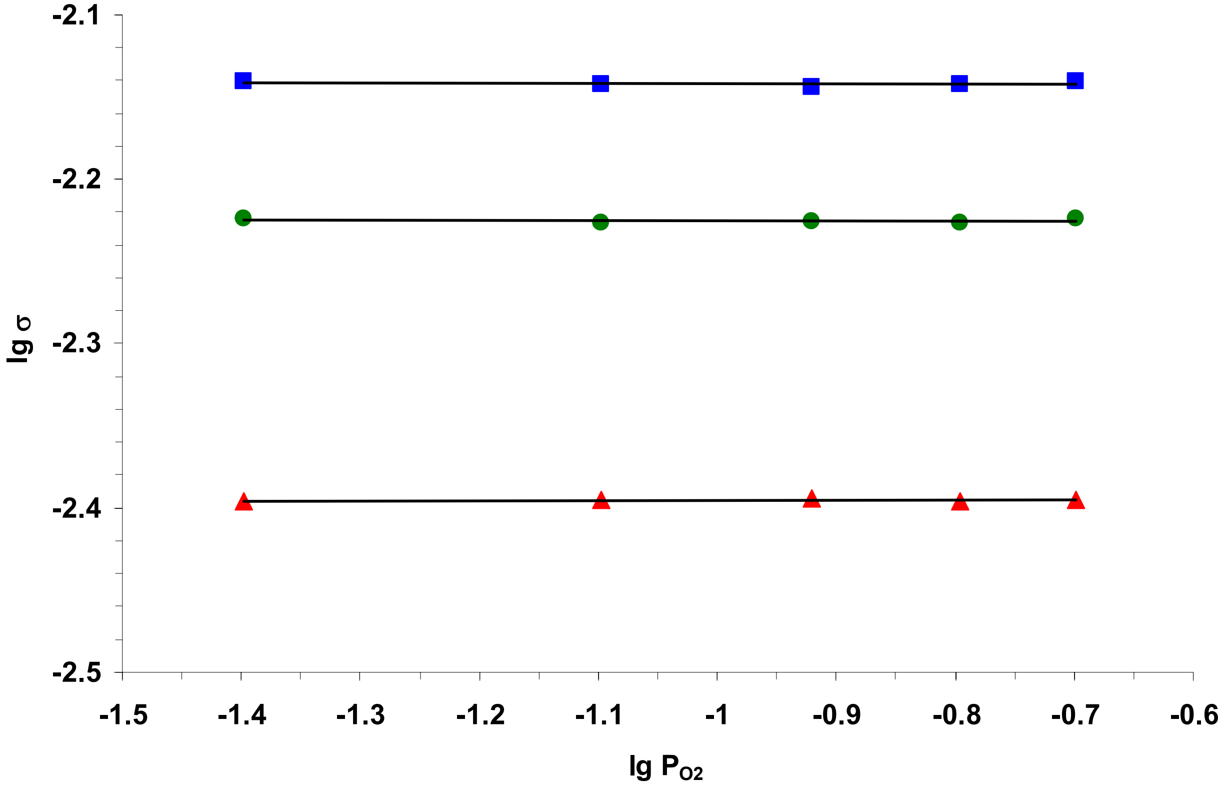

Figure 5.

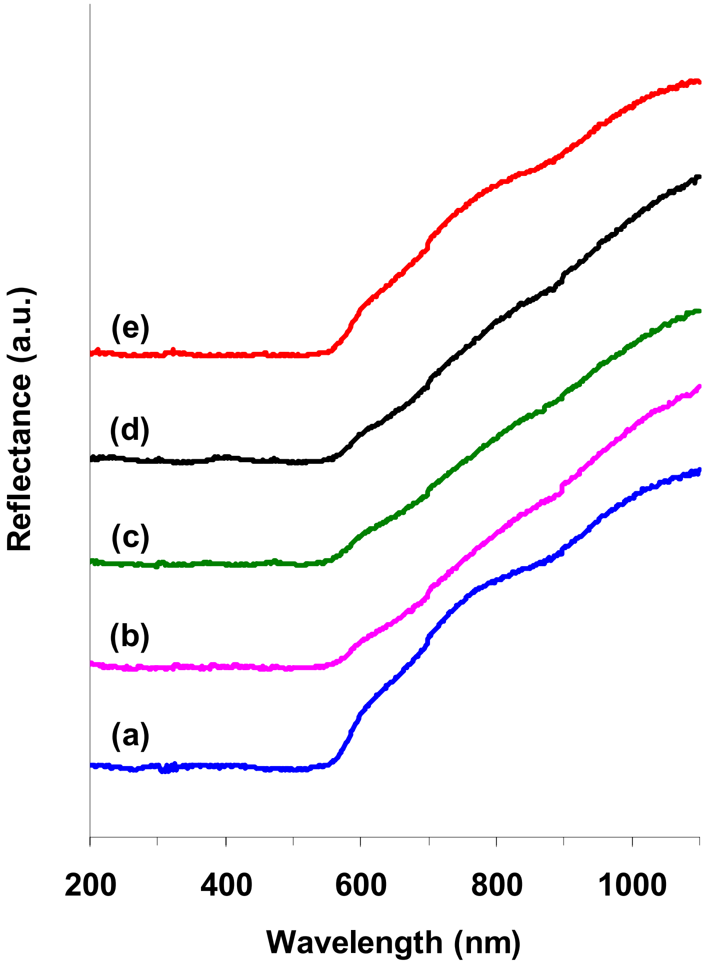

Figure 6.

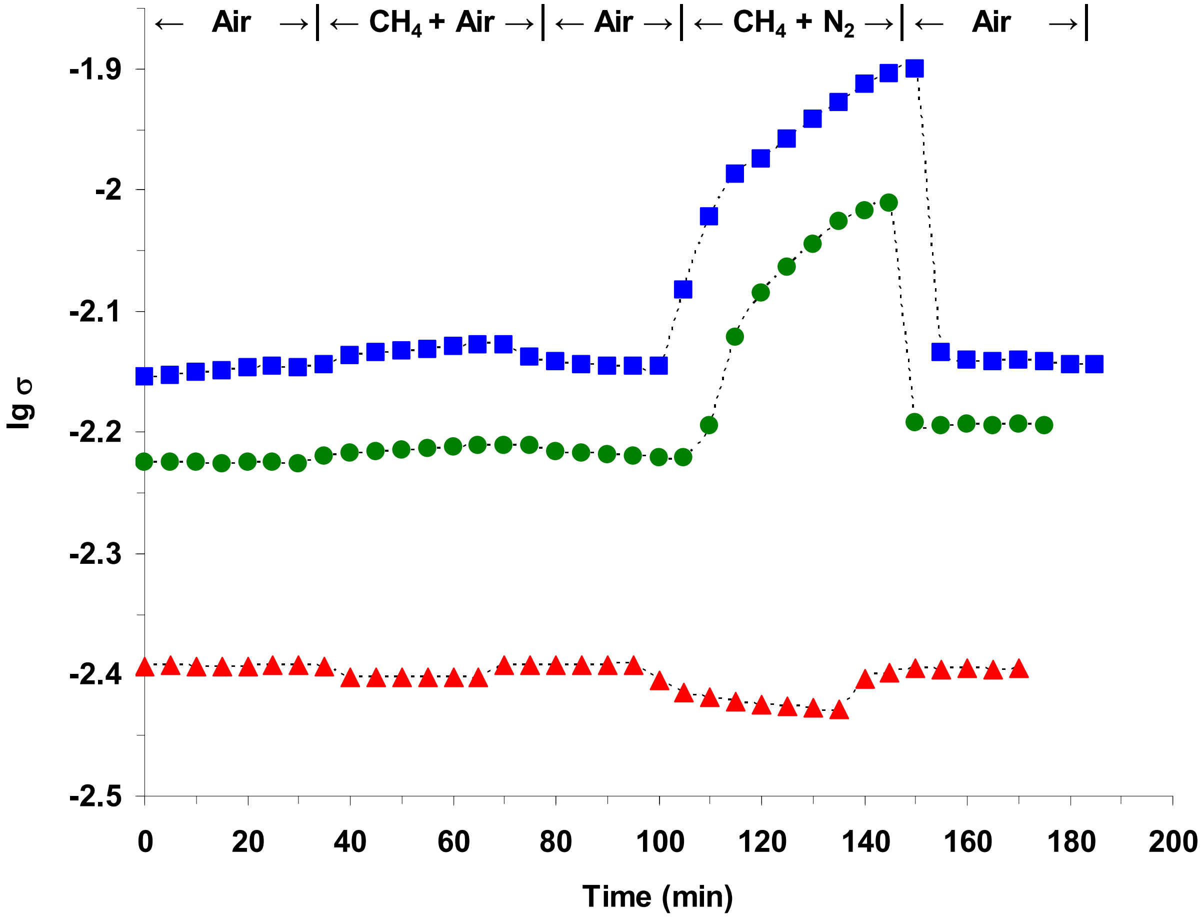
← Air →| ← CH₄ + Air →| ← Air →| ← CH₄ + N₂ →| ← Air →|
lg σ
-1.9
-2
-2.1
-2.2
-2.3
-2.4
-2.5
0
20
40
60
80
100
120
140
160
180
200
Time (min)

Graphical abstract

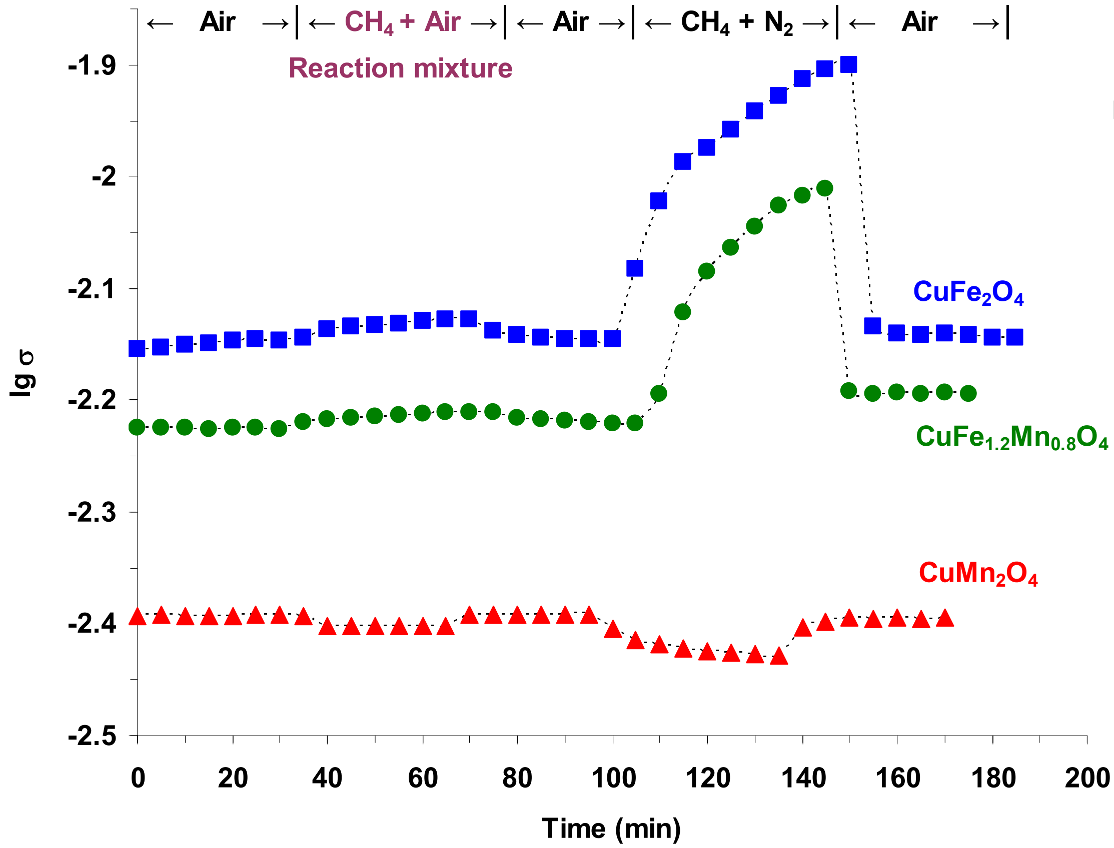

Popescu et al.

Research highlights

$CuFe_{2-x}Mn_xO_4$ spinels are catalysts for the total oxidation of methane.

The activity decreased with increasing the Mn content.

All the solids show both p-type and n-type semiconductivity.

All the spinels were partially reduced during catalysis.

All the catalysts are functioning via a heterogeneous redox mechanism.